Controlled Helical Propulsion Against the Flow of a Physiological Fluid

Chuang Li[1], Frank R. Halfwerk[2,3], Jutta Arens[2], Sarthak Misra[1,2], Michiel Warlé[4], and Islam S. M. Khalil[2]

***Abstract*— Untethered helical magnetic devices (UHMDs) have the potential to navigate bodily fluids using permanent-magnet robotic systems for minimally invasive diagnostic and surgical procedures. These devices can be actuated by robotically moving rotating permanent magnets (RPMs) to achieve controllable steering and propulsion simultaneously in a wireless manner. To date, the vast majority of motion control systems using UHMDs are constrained to operate in the absence of a dynamic flow field and prior work did not rigorously address the fundamental roles of rheological, magnetic, and geometric characteristics of the UHMD and its surroundings on the resulting stability. In this work, we show how to construct the region of attraction of a UHMD driven by two synchronized RPMs inside fluid-filled lumen around an equilibrium point. We first present the governing hydrodynamic model of a magnetically-driven UHMD to describe its behavior against the flow of blood serum. Then we validate the model using 1-D frequency response characterization and show that it captures the measured linear relationship between the actuation frequency and propulsive thrust at various flow fields. We find that a region of asymptotic stability can be achieved around an equilibrium point allowing a 6-mm-long UHMD to overcome maximum volumetric flow field of 1.2 l/hr (i.e., 2.65 cm/s).**

I. INTRODUCTION

There is an increasing clinical need for wireless untethered magnetic devices (UMDs) that can perform important functions such as sensing, diagnosis, locomotion, actuation, fluidic manipulation, material removal, and localized drug delivery [1], [2]. In particular, the use of untethered helical magnetic devices (UHMDs) and microrobots in biomedical applications is a promising method to move wirelessly toward inaccessible regions in the body. A great deal of research has addressed the potential of these devices in static-fluid environments to characterize their behavior and enhance their locomotion strategies [3]–[6]. However, motion control of these devices *in vivo* would require them to bypass the following hurdles: first, to swim controllably along and against the flow of bodily fluids inside confined environments [7]; second, to maintain proper locomotion conditions (i.e., generating enough propulsive thrust and remaining in sync with the external field) inside physiological fluids with heterogeneous rheological properties, near wall-effects, and concentrated cells; third, to be able to swim and drill through bodily fluids and soft-tissue, respectively, enabling interventions with large proportions of the body; and last, to scale up the magnetic manipulation system to the size of an intended biomedical application such as blood clot removal.

We see in the literature that the most promising magnetic manipulation approach is one where a controlled magnetic field is generated either using a clinical magnetic resonance imaging (MRI) system or by robotically moving a continuously rotating dipole field [8]–[11]. Some approaches produce controlled magnetic fields using configurations of electromagnets surrounding a workspace [12]. These configurations are mostly closed to compensate for the field that changes rapidly in space, resulting in a limited workspace suitable for *in vivo* small animal experiments only. An advantage of a clinical MRI system over any other magnetic manipulation system is their ability to simultaneously actuate and localize UMDs. However, the challenge is in the motion control of UHMDs that requires manipulation of its field-rotation axis and continuously rotating the magnetic field about this axis. An MRI system cannot control the direction of the magnetic field, thereby explicitly limiting the types of UMDs to those driven my magnetic field gradients.

If alternatively a permanent magnet (or multiple) is allowed to robotically move while rotating about a desired axis of rotation, then the magnetic force and torque can be managed to actuate and steer any type UMDs or UHMDs. For example, the permanent-magnet robotic system of Mahoney *et al.* works by controlling a single rotating permanent magnet (RPM) using a robotic manipulator to manage the magnetic force and torque in a wireless fashion [13]. They have demonstrated this method by actuating rotating magnetic devices in a lumen (i.e., spherical rolling UMD and UHMD). Instead of surrounding the workspace with a closed configuration of electromagnetic coils for controlled magnetic field generation [12], permanent-magnet robotic systems allow the RPM to move freely during wireless actuation of the UMDs. Niedert *et al.* have used this concept to control a tumbling UMD using a two-degree-of-freedom (DOF) rotating permanent magnet inside a murine colon *in vivo* [14]. However, the challenge is in the actuation of UMDs controllably in physiological flow conditions; that is, they must move in a wide range of flow rates with Reynolds number in the range 10-4000 [15]. In this work, we study the closed-loop motion characteristics of an externally actuated UHMD inside a physiological fluid-filled lumen with a dynamic flow. We begin by providing a

[1]C. Li and S. Misra are with the Department of Biomedical Engineering, University of Groningen and University Medical Center Groningen, 9713 GZ Groningen, The Netherlands.

[2]F. R. Halfwerk, J. Arens, S. Misra, and I. S. M. Khalil are with the Department of, Biomechanical Engineering, University of Twente, 7500 AE Enschede, The Netherlands (e-mail: i.s.m.khalil@utwente.nl).

[3]The author is with Thoraxcentrum Twente, Medisch Spectrum Twente, 7500 KA Enschede, The Netherlands.

[4]M. Warlé is with Radboud University Medical Center, 6525 GA Nijmegen, The Netherlands.

This work is supported by the European Research Council (ERC) under the European Unions Horizon 2020 Research and Innovation programme under Grant 866494 project-MAESTRO, and financial support from the China Scholarship Council (CSC).

978-1-6654-5973-0/22/$31.00 ©2022 IEEE

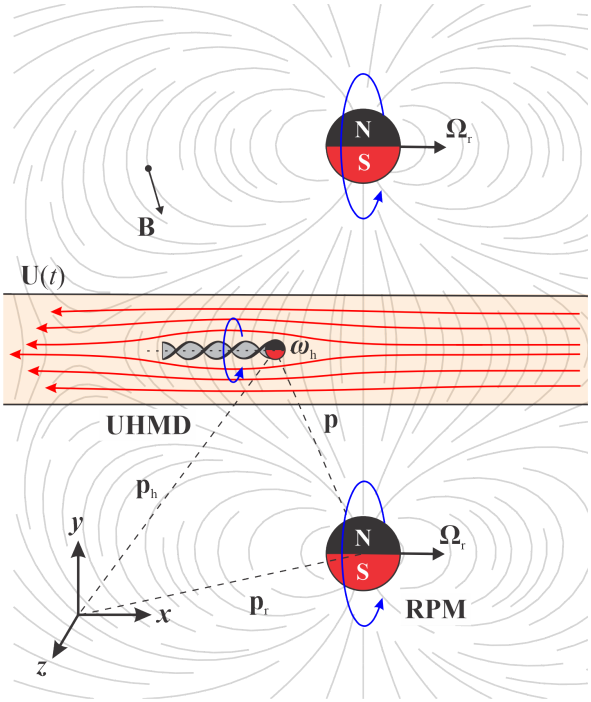

Fig. 1: An untethered helical magnetic device (UHMD) swims inside a fluid-filled lumen against the flow, $\mathbf{U}(t)$. Two rotating permanent magnets (RPMs) produce a time-periodic magnetic field, $\mathbf{B}$, applying magnetic torque on the magnetic moment of the UHMD. The UHMD and the RPMs are characterized by the position vectors $\mathbf{p}_{\mathrm{h}}$ and $\mathbf{p}_{\mathrm{r}}$, respectively. The UHMD can be steered by controlling the RPM's rotation axis, $\widehat{\mathbf{\Omega}}_{\mathrm{r}}$, robotically. To align the UHMD along the lumen, we set $\widehat{\mathbf{\Omega}}_{\mathrm{r}} = [1, 0, 0]^T$ with respect to frame of reference $\{\boldsymbol{x}, \boldsymbol{y}, \boldsymbol{z}\}$.

hydrodynamic model for the UHMD and estimate the size of the region of attraction around a desired reference position. Using the region of attraction enables us to understand the response of a UHMD to a wide range of flow rates and actuation frequencies. The problem of finding an open-loop equilibrium point and a region of attraction enables one-dimensional (1-D) control of the UHMD against the flow without feedback. The remainder of this paper is organized as follows: In Section II we give a brief overview of the governing equations of a UHMD to explain the basic properties of flow, interactions, and actuation. Characterization of the helical propulsion and 1-D control experiments are presented in Section III. Finally, Section IV concludes and provides directions for our future work.

II. LOCOMOTION OF HELICAL MAGNETIC DEVICES INSIDE FLUID-FILLED LUMEN

We consider a UHMD with an axis of symmetry $\widehat{\boldsymbol{\omega}}_{\mathrm{h}}$. The UHMD of length L and diameter $2R$ has an average magnetic moment $\mathbf{m}$, lying orthogonal to its axis of symmetry (i.e., $\mathbf{m}_{\mathrm{h}}^T \widehat{\boldsymbol{\omega}}_{\mathrm{h}} = 0$). The material frame of reference of the UHMD is located at its center of mass and characterized by the position vector $\mathbf{p}_{\mathrm{h}}$ with respect to a reference frame (Fig. 1). When the UHMD is placed between two synchronized RPMs with an average magnetic moment $\mathbf{M}$, it experiences a time-periodic magnetic field $\mathbf{B}(t, \mathbf{p})$. The magnetic field is nonuniform and not force free with the exception of the region between the RPMs [16]. These RPMs are robotically moved to control the rotation axis, $\widehat{\mathbf{\Omega}}_{\mathrm{r}}$, of the RPM and actuate the UHMD, while immersed in an inertial physiological fluid contained in a lumen. As the UHMD rotates about $\widehat{\boldsymbol{\omega}}_{\mathrm{h}}$, it swims against or along fluid flow $\mathbf{U}(t)$.

A. Governing Equations

We now develop the governing equations and discuss the theoretical background pertaining to the swimming scheme in Fig. 1. The two RPMs, which rotate in sync, are separated by equal distances to a fluid-filled lumen to assist the actuation of the UHMD by a resultant pulling magnetic force. When the RPMs are allowed to rotate about $\widehat{\mathbf{\Omega}}_{\mathrm{r}}$ while their position vector $\mathbf{p}_{\mathrm{r}}$ is kept fixed, the pulling magnetic force is expected to assist the propulsive thrust only in one part of the lumen. Consider, for example, the situation where the RPMs are located halfway along the lumen, then the position of the UHMD with respect to the RPM dictates the direction of the pulling magnetic force along the $\boldsymbol{x}$-axis. In the case when the UHMD is located halfway along the lumen between the RPMs, we will obtain a magnetic force to assist propulsion. This force is given by $\mathbf{f}_{\mathrm{m}} = (\mathbf{m} \cdot \nabla)\mathbf{B}(t, \mathbf{p})$ and counterbalances the fluidic drag force $\mathbf{f}_{\mathrm{d}} = 0.5\rho A C_{\mathrm{d}}(\mathbf{v} - \mathbf{U}(t))^2$, where $\mathbf{v}$ is the transnational velocity of the UHMD and A is its cross-sectional area. Further, ρ is the density of the fluid and C_{d} is the fluid dynamic resistance coefficient. When the UHMD rotates in sync with the RPMs, a propulsive thrust, $\mathbf{f}_{\mathrm{p}} = k\boldsymbol{\omega}$, would contribute to its transnational velocity regardless of its position with respect to the RPMs. Therefore, the total forces on the UHMD with a mass m is given by [17]

$$m\dot{\mathbf{v}} = \mathbf{f}_{\mathrm{m}} + \mathbf{f}_{\mathrm{d}} + \mathbf{f}_{\mathrm{p}} + \mathbf{f}_{\mathrm{c}} + \mathbf{f}_{\mathrm{w}}, \qquad (1)$$

where $\mathbf{f}_{\mathrm{c}}$ and $\mathbf{f}_{\mathrm{w}}$ are the contact forces with the wall of the lumen and apparent weight of the UHMD, respectively. Equation (1) completes the governing dynamics of the transnational motion and the rotational dynamics can be determined in a similar manner. Note that the basic properties of the flow dictates the importance of the inertial force in the left-hand side of Equation (1). Here, we are concerned with dynamic flow fields, $\|\mathbf{U}\| \sim 10^{-2}$ m/s and our UHMD in the millimeter range, yielding Reynolds number on the order $Re \sim 10$. Therefore, the interactions between the fluid's inertia and the viscous forces cannot be ignored and the contribution of the inertial force is incorporated in the numerical analysis.

B. Numerical Solution of the 1-D Problem

Researchers have explored numerical solutions for Equation (1) to predict the time-averaged forces and swimming trajectories. One very good way to gain more physical insight into the dynamics is to analyze the 1-D problem; perhaps the understanding can be used in a generalization for the full-order system. For 1-D swimming problem in the absence of

TABLE I: The untethered helical magnetic device (UHMD) contains a cylinderical Grade-N42 NdFeB magnet with magnetic moment $\mathbf{m}$. The rotating permanent magnet (RPM) is a cylinderical Grade-N52 NdFeB magnet with magnetic moment $\mathbf{M}$. Blood serum, of viscosity η and density ρ, is contained inside a cylindrical lumen of diameter $D_{\rm l}$ parallel to the rotation axis of the RPM, $\widehat{\boldsymbol{\Omega}}_{\rm r}$.

	Property	Value	Property	Value
UHMD	$2R \times L$ [mm]	1.5×6	$\Vert\mathbf{m}\Vert$ [A.m^2]	6.23×10^{-4}
	Pitch [mm]	1	Helicity [°]	71
RPM	$D \times H$ [mm]	45×30	M [A.m^2]	52.26
	$\widehat{\boldsymbol{\Omega}}_{\rm r}^T$	$[1, 0, 0]$	$\mathbf{B}$ [mT]	5
Fluid	ρ [kg.m^{-3}]	906	η [mPa.s]	1.105
	Re	< 10	$C_{\rm d}$	0.02
	$D_{\rm l}$ [mm]	4	$\Vert\mathbf{U}\Vert$ [ml/hr]	≤ 1200

contact, Equation (1) becomes simply

$$\begin{aligned} \dot{x}_1 &= x_2 \\ \dot{x}_2 &= 1/m \left(f_{{\rm m},x} + f_{{\rm d},x} + f_{{\rm p},x}\right), \end{aligned} \qquad (2)$$

where $f_{{\rm m},x}$, $f_{{\rm d},x}$, and $f_{{\rm p},x}$ are the force components along the $\boldsymbol{x}$-axis. Further, the states x_1 and x_2 represent the position and velocity components of the UHMD along the $\boldsymbol{x}$-axis, respectively. Physically, the magnetic force scales as $f_{\rm m} \sim 3\mu_0\Vert\mathbf{m}\Vert\Vert\mathbf{M}\Vert/2\pi x_1^4$, where μ_0 is the permeability of free space. Note that $f_{\rm m}$ changes sign with x_1, and qualitatively the contribution of the magnetic force is not expected to assist propulsion when the UHMD swims past the RPMs. Also since the UHMD and the surrounding fluids have non-zero velocities, the drag force scales with the velocity difference as $f_{\rm d} \sim (x_2 - U_x)^2$. Therefore, for a given flow rate, U_x, the drag force is quadratic in x_2. Finally, the propulsive thrust is linear in $\boldsymbol{\omega}$ of the UHMD, and subsequently linear in $\boldsymbol{\Omega}$ of the RPM, below a step-out frequency. Note that unlike the magnetic force and drag force, whose interactions with the states depends on the inverse fourth power of the position and second power of the velocity, the propulsive thrust can be controlled through the angular velocity of the RPMs.

Let us construct the phase portrait of the 1-D model using Equation (2) and the nominal parameters in Table 1. In this case, the RPM's rotation axis is set to $\widehat{\boldsymbol{\Omega}}_{\rm r} = [1, 0, 0]^T$ resulting in approximately 1-D swimming along the $\boldsymbol{x}$-axis of the lumen. Fig. 2 shows the constructed phase portrait when the flow field is set to $\Vert\mathbf{U}\Vert = 1200$ ml/hr and the angular frequency of the RPMs is 10 Hz. Inspection of the phase portrait shows that all trajectories starting in the interval $[0, L_1/2)$ cannot stay in the same interval. Although the UHMD continuously rotates about its axis of symmetry, it cannot move against the attractive magnetic force of the RPMs and the fluid drag. In contrast, trajectories of the UHMD starting in the interval $(-L_1/2, 0]$ will stay in the same interval for all future time. The trajectories spiral around an equilibrium point (red circle) and cannot stay identically in any of the closed sets that are shown by the blue curves.

All trajectories in the set $S = \{x_1 < 0, |x_2| > 0\}$ will spiral around the equilibrium point along asymmetric closed curves. This asymmetric pattern is attributed to the

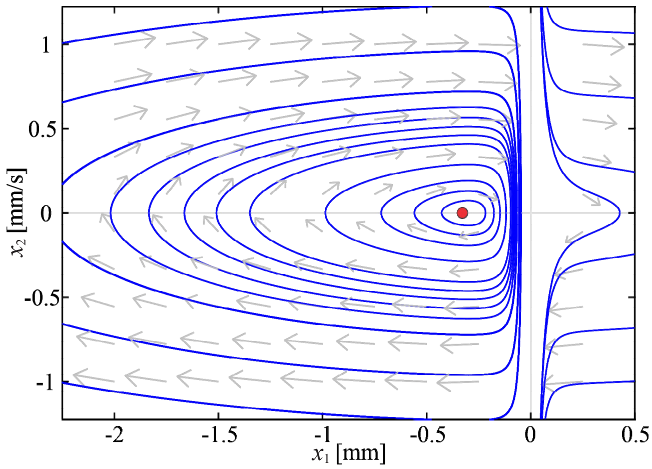

Fig. 2: Inspection of the phase portrait of the 1-D hydrodynamics of the UHMD shows that trajectories of the states, $[x_1, x_2]^T$, starting in the interval $[0, L_{\rm l}/2)$ cannot stay in the same interval because the flow and the pulling magnetic force act along the same direction (negative $\boldsymbol{x}$-axis). In the interval $(-L_{\rm l}/2, 0]$, where the magnetic force is opposite to the flow, the UHMD can stay within a region centered at the equilibrium point (red circle). $L_{\rm l}$ represents the total length of the lumen.

nonlinearity of all forces in Equation (2) with the exception of the propulsive thrust. The component of the pulling magnetic force along the $\boldsymbol{x}$-axis increases as the inverse fourth power of the position and falls off rapidly when the UHMD swims from left to right toward the region between the RPMs where the magnetic field is more uniform. Within this region, the field is more uniform than that of any other positions along the lumen and the magnetic force vanishes by the symmetry of the RPMs with respect to the lumen and the UHMD. Therefore, a UHMD with trajectories starting in the set S will oscillate and remain in one of the blue closed curves in Fig. 2 only if all conditions remain *ideally* fixed.

Note that the oscillation of the states of the UHMD is a result of energy transfer between the kinetic energy storage elements (i.e., inertia of the fluid and the UHMD) and the potential energy storage element (i.e., magnetic field). The amplitude of this oscillation is dependent on the initial conditions and the system can have a steady-state oscillation with a small amplitude around the equilibrium point. In this case, the propulsive thrust and the pulling magnetic force will hold the UHMD against the flow, but will not allow it to swim far beyond the set S. This problem can be alleviated if the RPMs are translated along the lumen, and permanent-magnet robotic systems are typically equipped with transnational DOF that can be employed to shift the equilibrium point along a prescribed path in an open-loop fashion.

III. MAGNETIC ACTUATION AND MOTION CONTROL AGAINST THE FLOW

In our experiments, a permanent-magnet robotic system is used to generate controlled rotating magnetic field to validate the results of the 1-D model. The position of the RPMs is kept fixed with respect to the lumen, as shown in Fig. 1.

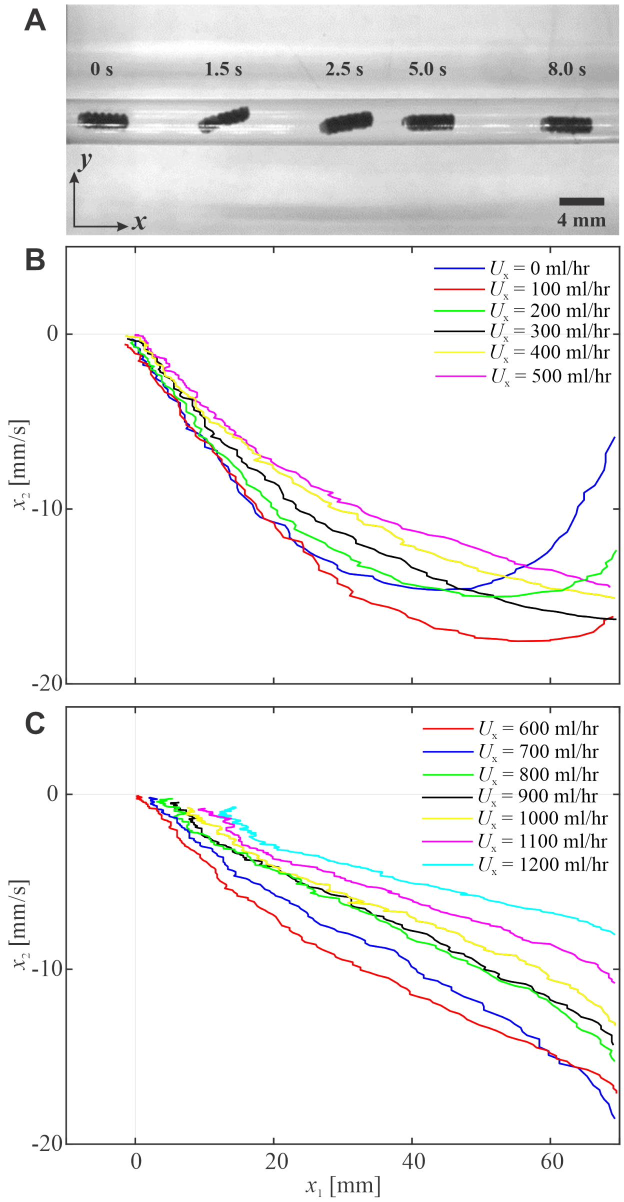

Fig. 3: Open-loop control of a UHMD against the blood serum flow. The UHMD swims from left to right at $\boldsymbol{\omega} = 10$ Hz. (A) The UHMD is attracted toward the equilibrium point at zero flow. (B)-(C) Convergence of the states for the flow range of $0 \leq \|\mathbf{U}\| \leq 500$ and $600 \leq \|\mathbf{U}\| \leq 1200$ ml/hr. *Please refer to the accompanying video.*

A. Experimental Results

A lumen of 4 mm in diameter by 70 mm long is connected to a pump system (77910-55 L/S Variable-Speed Pump System, Masterflex, Illinois, USA) to regulate the flow of blood serum (F7524–500ML, Sigma-Aldrich, USA). The diameter of the lumen is comparable to the medium arteries and veins. Flow measurements inside the lumen are conducted using an ultrasound system (SonixTouch Q+, BK Medical, Quickborn, Germany). The lumen is placed in the $\boldsymbol{xy}$-plane to lie parallel to the $\boldsymbol{x}$-axis between the RPMs of the permanent-magnet robotic system (Fig. 1). The long axis of the lumen and the rotation axes of the RPMs are constrained to lie in the $\boldsymbol{xy}$-plane. A UHMD of 6 mm in

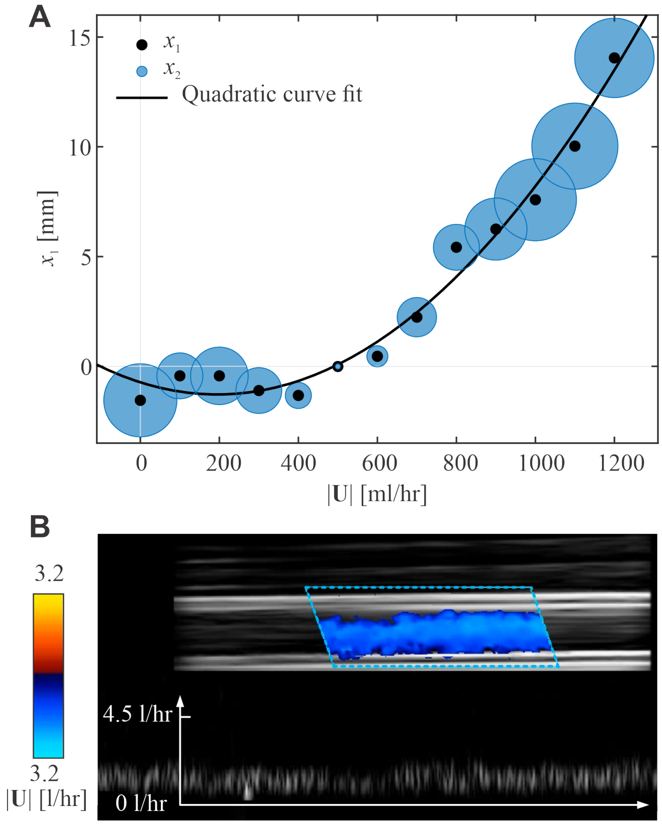

Fig. 4: The equilibrium point, (x_1, x_2), shifts approximately quadratically with the flow rate, $\|\mathbf{U}\|$. (A) The size of the bubble represents the measured x_2-component of the equilibrium point. (B) The flow rate of blood serum is visualized and measured using Doppler data. Gelatin is used as phantom to contain the lumen with respect to the transducer at depth of 2.5 cm.

length and 1.5 mm in diameter is 3-D printed using polylactic acid and assembled to a cylinder of NdBFe magnet such that the magnetic moment is perpendicular to the long axis of the helical body (pitch of 1 mm). The NdBFe magnet is 1 mm in length and diameter and provides an average magnetic moment of 6.23×10^{-4} A.m^2.

B. Open-Loop Characterization of the Region of Attraction

Below the setp-out frequency of the UHMD, its propulsive thrust is linearly proportional to its angular velocity, $\boldsymbol{\omega}$. This is the rotational velocity at which the UHMD will trail behind the rotating magnetic field of the two RPMs. We allow the RPMs to rotate in synchrony at an angular frequency of $\|\boldsymbol{\Omega}\| = 10$ Hz. In this experiment, the UHMD is initially located at one side of the lumen and allowed to swim from left to right. This is equivalent to the numerical results by setting the initial states of the UHMD to the set S. Blood serum is allowed to flow along the $-\boldsymbol{x}$-axis (from right to left) in the $0 \leq \|\mathbf{U}\| \leq 1200$ range. At $\|\mathbf{U}\| = 0$ ml/hr, the UHMD is propelled and pulled toward the open-loop equilibrium point, as shown in Fig. 3(A). Note that, at $t = 8$ s, the UHMD reaches the equilibrium point and its states become close to zero (Fig. 3(B)). When flow is induced for the same actuation inputs, the equilibrium point slightly shifts, as shown in Figs. 3(B) and 3(C).

To understand the significance of the flow rate, we can determine the equilibrium point in the uniform field region between the RPMs. By setting $\dot{x}_1 = \dot{x}_2 = 0$, and solve for x_1 and x_2, we have

$$(x_1, x_2) = \left(\frac{\rho A C_\mathrm{d}}{2k} \|\mathbf{U}\|^2, 0 \right). \tag{3}$$

When the fluid is static (i.e., $\|\mathbf{U}\| = 0$), the equilibrium point is at the origin, $(x_1, x_2) = (0, 0)$. For a non-zero flow, the equilibrium points shifts quadratically with $\|\mathbf{U}\|$ along the x_1-axis. Note that the average magnetic moments of the UHMD and the RPM do not play a role in the equilibrium point because it is located in the uniform field region. Therefore, the location of the equilibrium point depends only on the characteristics of the flow, geometric parameters of the UHMD, and the relationship between the propulsive thrust and the angular velocity. Using the same open-loop data set in Fig. 3, we can investigate the steady-state response of each trajectory versus each flow rate. Fig. 4 shows the location of each equilibrium point for a given flow field. The bubble size specify the x_2-component of the equilibrium point. We see that the x_1-component shifts approximately quadratically with $\|\mathbf{U}\|$, and therefore the equilibrium point (3) captures the experimental behavior of the UHMD during helical propulsion against the flow in the $600 \leq \|\mathbf{U}\| \leq 1200$ ml/hr range. It is desirable to decrease the influence of the flow rate on the location of the equilibrium point. Once the UHMD moves and approaches the equilibrium point, the behavior of the trajectories around the equilibrium point will depend on (3). This implies that when the UHMD is close enough to the equilibrium point, the geometric and rheolgical characteristics of the UHMD and the flow will only scale the effect of the flow. A smaller cross-sectional area, leads to a smaller shift in the equilibrium point regardless of the induced flow. Similarly, a steep frequency response curve (i.e., greater k), leads also to smaller shifts in the equilibrium. Finally, flow characterized with greater Re will lead to smaller C_d, resulting in smaller shift in the equilibrium point.

C. Asymptotic Regulation Against Flow

Suppose we can control the angular velocity of the RPM such that a desired state feedback control law stabilizes the equilibrium point. Setting $f_{p,x} = k_1 x_1 + k_2 x_2$ in Equation (2) yields a stable equilibrium point, as shown in Fig 5. Once again notice that all trajectories starting outside the set S would not stay in S. However, if we restrict the trajectories to start in S they will spiral toward the origin. The red and black trajectories indicate two different sets of initial conditions, both starting in S. Note that the phase portraits in Fig. 2 and Fig. 5 differ from each other in that the trajectories will not converge asymptotically in the case of open-loop actuation against the flow, while convergence to the equilibrium point is achieved when the angular velocity of the RPMs is applied as a function of the states of the UHMD.

Now we implement this asymptotic regulation strategy as before for the same flow range. Fig. 6(A) shows the

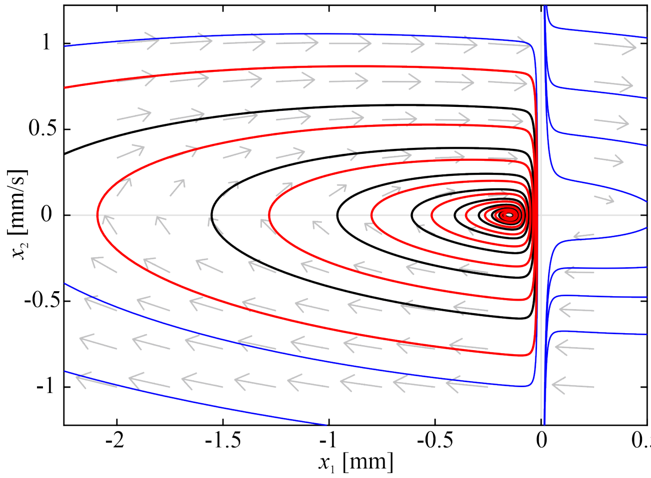

Fig. 5: Phase portrait of the 1-D hydrodynamics of the UHMD with state feedback control shows a stable equilibrium point. The black and red trajectories indicate two different sets of initial conditions starting in the interval $(-L_1/2, 0]$. These trajectories spiral toward the equilibrium point. Length of the lumen is L_1.

motion of the UHMD from left to right toward a reference position (red circle). In this trial, the UHMD is controlled against fluid flow of 1200 ml/hr. At $t = 15$ s, the UHMD is fixed with respect to the reference position. As the UHMD approaches the reference position, the pulling magnetic force decreases and becomes dependent on its propulsive thrust only. At this time instant, the propulsive thrust is large enough to hold the UHMD against the flow but insufficient to reach the target. In this case the position tracking error is measured as 2 body lengths (i.e., 12 mm).

Figs. 6(B) and 6(C) show the closed-loop behavior of the UHMD for the flow range of $0 \leq \|\mathbf{U}\| \leq 1200$. In this range the error in absolute value is bounded by 2 body lengths and decreases to approximately 0.1 body length (i.e., 1 mm) when the flow rate is decreased to zero. There is a close agreement between the phase portrait (Fig. 5) and the results of this closed-loop control trial (Fig. 6) in that the UHMD converges to the equilibrium point as t tends to infinity. The location of the equilibrium point shifts as a function of the flow rate, as shown in Fig. 4(A), allowing us to predict the stead-state error for a given flow rate.

Analysis of the phase portraits of the open- and closed-loop equilibria show that a state feedback input is required to achieve convergence of the trajectories. While the trajectories of the open-loop system will not approach the equilibrium, exhibiting oscillatory response with unsustained amplitude, the need to hold the UHMD within a region around the equilibrium point might be useful when feedback is not available. Note that the fluid flow is restricted to be uniform in our analysis and experiments, as shown in Fig 4(B). A pulsatile flow is not likely to yield significant difference in the behavior since a pulling magnetic force assists the propulsive thrust in fixing the UHMD around the equilibrium point. A pulsatile flow can be considered in Equation (2) as a uniformly bounded periodic disturbance (i.e., there exists

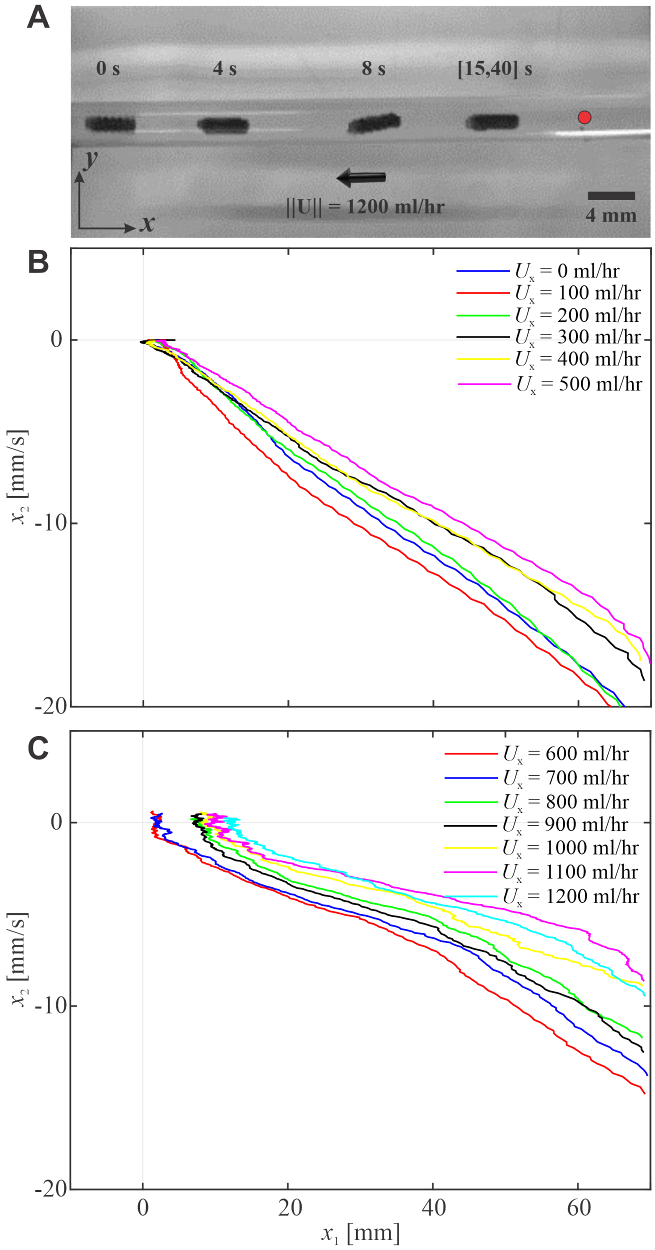

Fig. 6: Closed-loop control of a UHMD against the blood serum flow. (A) The UHMD swims from left to right against flow of 1200 ml/hr toward the reference position (red circle). (B)-(C) Convergence of the states for the flow range of $0 \leq \|\mathbf{U}\| \leq 500$ and $600 \leq \|\mathbf{U}\| \leq 1200$ ml/hr. *Please refer to the accompanying video.*

$c > 0$, such that $\|f_{\mathrm{d},x}\| \leq c$, $\forall t \geq 0$). With the uniform boundendeness of the pulsatile drag, the control problem becomes one of finding a state feedback control law to achieve exponential stability of the system with zero flow.

IV. Conclusions

We provide a 1-D model for the helical propulsion of an externally actuated UHMD against blood serum. This model provides an open-loop equilibrium point, in the uniform field region between two RPMs, that shifts quadratically with the flow. We test the open- and closed-loop behavior using this model and show that we can achieve asymptotic convergence against maximum flow rate of 1200 ml/hr. At this flow rate, the error in absolute value is bounded by 2 body lengths and reduces significantly to 0.1 body length when the flow is decreased to zero. The gained physical insights and correspondence between theoretical and experimental results motivates the use of our system to test UHMDs in clinical physiological flow conditions in future research.

References

[1] B. J. Nelson, I. K. Kaliakatsos, and J. J. Abbott, “Microrobots for minimally invasive medicine,” *Annual Review of Biomedical Engineering*, vol. 12, pp. 55–85, 2010.

[2] M. Sitti, H. Ceylan, W. Hu, J. Giltinan, M. Turan, S. Yim, and E. Diller, “Biomedical applications of untethered mobile milli/microrobots,” *Proceedings of the IEEE*, vol. 103, no. 2, pp. 205–224, 2015.

[3] A. Ghosh and P. Fischer, “Controlled propulsion of artificial magnetic nanostructured propellers,” *Nano Letters*, vol. 9, no. 6, pp. 2243–2245, 2009.

[4] L. Zhang, T. Petit, Y. Lu, B. E. Kratochvil, K. E. Peyer, R. Pei, J. Lou, and B. J. Nelson, “Controlled propulsion and cargo transport of rotating nickel nanowires near a patterned solid surface,” *ACS Nano*, vol. 4, no. 10, pp. 6228–6234, 2010.

[5] S. Tottori, L. Zhang, F. Qiu, K. K. Krawczyk, A. Franco-Obregón, and B. J. Nelson, “Magnetic helical micromachines: fabrication, controlled swimming, and cargo transport,” *Advanced Materials*, vol. 24, no. 6, pp. 811–816, 2012.

[6] A. Servant, F. Qiu, M. Mazza, K. Kostarelos, and B. J. Nelson, “Controlled in vivo swimming of a swarm of bacteria-like microrobotic flagella,” *Advanced Materials*, vol. 27, no. 19, pp. 2981–2988, 2015.

[7] L. Arcese, M. Fruchard, and A. Ferreira, “Endovascular magnetically guided robots: navigation modeling and optimization,” *IEEE Transactions on Biomedical Engineering*, vol. 59, no. 4, pp. 977–987, 2011.

[8] J.-B. Mathieu, G. Beaudoin, and S. Martel, “Method of propulsion of a ferromagnetic core in the cardiovascular system through magnetic gradients generated by an mri system,” *IEEE Transactions on Biomedical Engineering*, vol. 53, no. 2, pp. 292–299, 2006.

[9] S. Martel, M. Mohammadi, O. Felfoul, Z. Lu, and P. Pouponneau, “Flagellated magnetotactic bacteria as controlled mri-trackable propulsion and steering systems for medical nanorobots operating in the human microvasculature,” *The International Journal of Robotics Research*, vol. 28, no. 4, pp. 571–582, 2009.

[10] T. W. Fountain, P. V. Kailat, and J. J. Abbott, “Wireless control of magnetic helical microrobots using a rotating-permanent-magnet manipulator,” in *Proceedings of the IEEE International Conference on Robotics and Automation (ICRA)*, 2010, pp. 576–581.

[11] A. W. Mahoney and J. J. Abbott, “Managing magnetic force applied to a magnetic device by a rotating dipole field,” *Applied Physics Letters*, vol. 99, no. 13, p. 134103, 2011.

[12] M. P. Kummer, J. J. Abbott, B. E. Kratochvil, R. Borer, A. Sengul, and B. J. Nelson, “Octomag: An electromagnetic system for 5-dof wireless micromanipulation,” *IEEE Transactions on Robotics*, vol. 26, no. 6, pp. 1006–1017, 2010.

[13] A. W. Mahoney and J. J. Abbott, “Generating rotating magnetic fields with a single permanent magnet for propulsion of untethered magnetic devices in a lumen,” *IEEE Transactions on Robotics*, vol. 30, no. 2, pp. 411–420, 2013.

[14] E. E. Niedert, C. Bi, G. Adam, E. Lambert, L. Solorio, C. J. Goergen, and D. J. Cappelleri, “A tumbling magnetic microrobot system for biomedical applications,” *Micromachines*, vol. 11, no. 9, p. 861, 2020.

[15] A. Mahalingam, U. U. Gawandalkar, G. Kini, A. Buradi, T. Araki, N. Ikeda, A. Nicolaides, J. R. Laird, L. Saba, and J. S. Suri, “Numerical analysis of the effect of turbulence transition on the hemodynamic parameters in human coronary arteries,” *Cardiovascular Diagnosis and Therapy*, vol. 6, no. 3, p. 208, 2016.

[16] A. Hosney, A. Klingner, S. Misra, and I. S. Khalil, “Propulsion and steering of helical magnetic microrobots using two synchronized rotating dipole fields in three-dimensional space,” in *Proceedings of the IEEE/RSJ International Conference on Intelligent Robots and Systems (IROS)*, 2015, pp. 1988–1993.

[17] L. Arcese, A. Cherry, M. Fruchard, and A. Ferreira, “Dynamic behavior investigation for trajectory control of a microrobot in blood vessels,” in *Proceedings of the IEEE/RSJ International Conference on Intelligent Robots and Systems (IROS)*, 2010, pp. 5774–5779.